Available online at www.sciencedirect.com

jmr&t Journal of Materials Research and Technology

journal homepage: www.elsevier.com/locate/jmrt

Original Article

On the relationship between the Raman scattering features and the Ti-related chemical states of $Ti_xO_yN_z$ films

A.R. Zanatta [a,*], F. Cemin [b], F.G. Echeverrigaray [b], F. Alvarez [b]

[a] Instituto de Física de São Carlos, USP, São Carlos, 13560-970, SP, Brazil
[b] Instituto de Física Gleb Wataghin, UNICAMP, Campinas, 13083-970, SP, Brazil

ARTICLE INFO

Article history:
Received 21 May 2021
Accepted 27 June 2021
Available online 7 July 2021

Keywords:
Titanium oxynitride ($Ti_xO_yN_z$)
Raman scattering
XPS spectroscopy

ABSTRACT

Owing to its singular and (to some extend) adaptable characteristics, titanium oxynitride ($Ti_xO_yN_z$) represents an exceptional choice in the realm of new materials aiming at the development of practical devices. However, the effective use of $Ti_xO_yN_z$ in photovoltaic and (photo)catalysis applications, for example, relies on a refined production–properties balance. Accordingly, this paper reports on the physico-chemical properties of $Ti_xO_yN_z$ films as investigated by means of the Raman scattering and X-ray photoelectron spectroscopy (XPS) techniques – the former shedding light on the structural characteristics of the films, and the latter providing the state of oxidation of the film's constituents. The films were prepared by sputtering TiO_2 and Ti targets in a plasma comprising different mixtures of Ar and N_2. Because of the deposition method and conditions, the films exhibit Raman spectra that are consistent with a combination of TiO_2 and TiN or, more properly, $Ti_xO_yN_z$ under the amorphous and (nano/micro-)crystalline structures. In fact, the experimental data indicate the presence of four TiO_2- and two TiN-related phonon modes, whose relative scattering features scale with the oxygen and nitrogen contents of the films. A similar concentration dependence was verified with the percentage of Ti^{4+}, Ti^{3+}, and Ti^{2+} chemical states of oxidation. This mutual concentration dependence was explored thoroughly and the results clearly indicate the suitability of the Raman data to estimate the typical atom composition and distribution of the Ti-related chemical states of $Ti_xO_yN_z$.

1. Introduction

For a long time, the optical-electronic characteristics of oxynitrides have attracted widespread attention from the scientific community [1]. Whereas part of this interest involved the study of their basic aspects (production, chemistry, etc.), several efforts have been focused on the development of oxynitrides with specific new-superior properties. Within this scenario, the titanium oxynitride $Ti_xO_yN_z$ occupies a privileged position and it is anticipated to produce considerable technological advances in the near future. Roughly, $Ti_xO_yN_z$ is a multicomponent material that, depending on its composition and

* Corresponding author.
E-mail address: zanatta@ifsc.usp.br (A.R. Zanatta).
https://doi.org/10.1016/j.jmrt.2021.06.090

structure, exhibits properties midway between those of TiO_2 and TiN. As a result, under suitable atomic arrangements, the properties of $Ti_xO_yN_z$ could expand the range – or even improve the performance – of applications typically performed by TiO_2 (such as in photovoltaics [2] and catalysis [3–5], for example), and TiN (hard coatings [6], plasmonics [7], and transparent conducting layers [8]).

With this in mind, $Ti_xO_yN_z$ has been prepared either by modifying its precursors – *i.e.*, nitrogen (oxygen) implantation of TiO_2 (TiN) or nitridation (oxidation) of TiO_2 (TiN) – or by constructing its structure "atom-by-atom" (as provided by physical- and/or chemical-based routes) [9]. Whatever the chosen preparation method (and conditions), understanding the basics behind the $Ti_xO_yN_z$ formation and, above all, controlling the $Ti_xO_yN_z$ characteristics are crucial for any practical application [4]. In fact, these have been the purposes of many works investigating the role played by different atomic compositions-structures [10,11], in close association with the presence of defects [12], onto the final properties of $Ti_xO_yN_z$. Therefore, allied to the successful preparation of $Ti_xO_yN_z$ it is important to assess its main properties to establish every possible cause-and-effect relationship. The Raman scattering and X-ray photoelectron spectroscopic techniques (in the middle of many others) perfectly meet this requirement by providing key physico-chemical information. Besides, they are well-established techniques that are available in most laboratories carrying out research in the field of materials science [13,14].

This forms the basis of this paper that reports on the structural and chemical characteristics of $Ti_xO_yN_z$ films as presented, respectively, by Raman and X-ray photoelectron spectroscopy measurements. The films were produced by sputtering TiO_2 and Ti targets with plasma atmospheres consisting of Ar + N_2 mixtures. The analysis of the Raman spectra indicates an amorphous + crystalline structure corresponding to TiO_2- and TiN-related phonon contributions that change with the oxygen and nitrogen concentrations of the $Ti_xO_yN_z$ films. A similar composition dependence was observed with the development of the Ti^{4+} (TiO_2-related), Ti^{3+} ($Ti_xO_yN_z$), and Ti^{2+} (TiN) chemical states of titanium. Altogether, the experimental results clearly indicate the importance of Raman scattering spectroscopy in evaluating the average atom composition and the Ti-related chemical states of $Ti_xO_yN_z$.

2. Experimental details

The $Ti_xO_yN_z$ films were deposited in a high-vacuum chamber (base pressure ~ 2×10^{-6} Torr) by sputtering TiO_2 and Ti solid targets onto fused silica and crystalline silicon substrates kept at 375 ± 25 °C. Each deposition run was 3 h long and it was assisted by a radio frequency (13.56 MHz) generated plasma obtained from a mixture of high-purity Ar and N_2 gases (constant total pressure of 10^{-4} Torr – as imposed by a vacuum throttle valve). As a result, a series of seven different $Ti_xO_yN_z$ films were produced (see Table 1).

After preparation, the atomic structure and chemical composition of the $Ti_xO_yN_z$ films were investigated by means of Raman scattering and X-ray photoelectron spectroscopy (XPS), respectively. All measurements were carried out at room-temperature and, in order to minimize either spurious signals or charging effects, they considered films deposited onto fused silica (Raman) and crystalline silicon (XPS) substrates. The Raman spectra were achieved with 632.8 nm photon excitation, backscattering geometry and no preferential polarization, rendering ~2 cm^{-1} resolution. The XPS measurements took place under ultra-high-vacuum conditions (~10^{-9} Torr) by using a monochromatic Al X-ray source (1486.6 eV and 50 meV linewidth) and no sample cleaning was performed. The XPS spectra were energy-corrected by the C 1s level (at 284.8 eV) and their analysis followed the standard procedure (*i.e.*, subtraction of electron inelastic scattering [15] and correction by sensitive factors [16]). Further study included the deconvolution of the Ti 2p (and N 1s and O 1s) core levels – according to their different chemical states and (where applicable) spin–orbit components – with Gaussian functions. In all cases, the CasaXPS processing software [17] was considered, providing the atom concentrations (Table 1) and the Ti-related chemical information.

3. Results

Fig. 1(a) shows the Raman spectra of some representative $Ti_xO_yN_z$ films. As can be seen, the scattering signals are rather broad indicating that the atomic structure of the films is amorphous or constituted by a mixture of amorphous + (nano/micro-)crystalline contributions [13]. Also, it is clear the influence of the deposition conditions (or chemical composition of the films) on the overall shape of the Raman spectra, in which the scattering signals at ~ 180 and 550 cm^{-1} develop with the nitrogen content of the films. A similar phenomenon can be observed in Fig. 1(b) that displays the XPS spectra of the Ti 2p core levels of the same $Ti_xO_yN_z$ films. In this case, however, the most prominent changes (as induced by the composition of the films) refer to the Ti^{3+} states, for example.

Table 1 – Main characteristics of the $Ti_xO_yN_z$ films: identification, deposition conditions (sputtering target and plasma atmosphere), and atom concentration (as determined from XPS measurements). sccm corresponds to *standard cubic centimeter*.

Sputtering target		Film A	Film B	Film C	Film D	Film E	Film F	Film G
		Ti	TiO_2	TiO_2	TiO_2	TiO_2	TiO_2	Ti
Plasma atmosp (sccm)	Ar	2.0	2.0	1.5	1.0	0.5	0.0	0.0
	N_2	0.0	0.0	0.5	1.0	1.5	2.0	2.0
Atom concentration (±2 at.%)	Ti	46	34	32	33	34	34	36
	O	54	65	49	45	39	37	24
	N	(0.6)	(1.0)	19	22	27	29	41

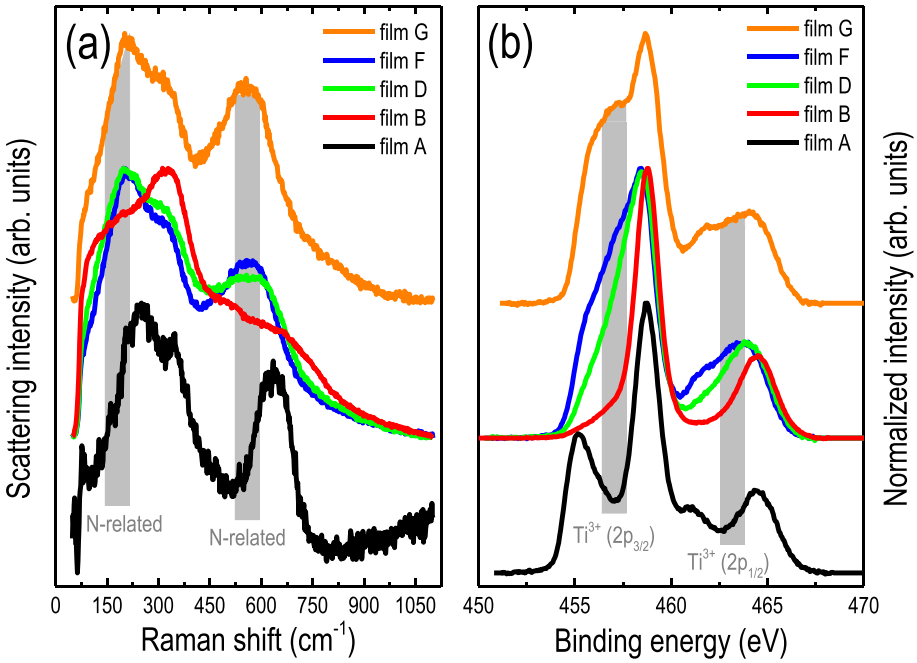

Fig. 1 – (a) Raman scattering spectra of some $Ti_xO_yN_z$ films produced by sputtering according to different deposition conditions (see Table 1). (b) Same as in (a) but concerning the XPS of the Ti 2p core levels. The spectra in (a) and in (b) were normalized and vertically shifted for comparison reasons.

The features present in Fig. 1 can be analyzed in detail by separating the experimental spectra according to their main constituents, *i.e.*: scattered light due to Ti–O and Ti–N bonds (Raman), and photoelectrons associated with the different Ti-related chemical states (XPS). In the first case, the Raman O- and N-related contributions were defined in view of their TiO_2 and TiN (either amorphous or crystalline) counterparts. According to literature, crystalline TiO_2 exists mainly in the Anatase and Rutile phases and presents Raman signals at approx. [18]: 144 cm^{-1} (corresponding to the Anatase-E_g and Rutile-B_{1g} vibration modes), 196 cm^{-1} (Anatase-E_g), 235 cm^{-1} (combination of Rutile modes), 395 cm^{-1} (Anatase-B_{1g}), 448 cm^{-1} (Rutile-E_g), 518 cm^{-1} (Anatase-A_{1g} + B_{1g}), 609 cm^{-1} (Rutile-A_{1g}), and 639 cm^{-1} (Anatase-E_g). These figures contrast with those of amorphous TiO_2 in which the scattering signals are red-shifted and considerably broader [19]. Regarding the Ti–N bonds, their phonon vibration modes could be either of acoustic (A), optical (O), longitudinal (L) or transversal (T) nature and, usually, take place at [20,21]: ~235 (TA), 320 (LA), 440 (2A), and 570 (TO). Besides, considering its small polarizability change (due to a face-centered cubic structure allied to the presence of nitrogen vacancies [20]), TiN is known to always present broad Raman signals – no matter its structure is amorphous or (nano/micro-)crystalline.

Based on these facts, and taking into account the amorphous character (resulting from the deposition method and conditions) of the samples and possible coupling of the TiO_2- and TiN-related phonons, the Raman spectra of the $Ti_xO_yN_z$ films were investigated thoroughly. In view of that, six major contributions – in the form of Gaussian functions – were achieved for $Ti_xO_yN_z$: four ascribed to TiO_2 (at ~ 110 ± 20, 300 ± 20, 430 ± 20, and 630 ± 20 cm^{-1}) and two related to TiN (at ~ 180 ± 15, and 550 ± 25 cm^{-1}). The main results of these TiO_2- and TiN-related phonon bands in some selected $Ti_xO_yN_z$ films are shown in Fig. 2(a)–(c)–(e). As can be seen, the proposed bands assignment is very descriptive and reproduces most of the Raman spectra with remarkable precision.

The analysis of the XPS spectra was performed essentially in terms of the Ti 2p core levels. In this case, the XPS spectra were deconvoluted according to the Ti^{4+}, Ti^{3+}, and Ti^{2+} chemical states and respective spin–orbit components (again in the form of Gaussian contributions), and the final results are presented in Fig. 2(b)–(d)–(f). Therefore, it was possible to obtain information regarding the chemical states of Ti that are typically attributed to [22,23]: (a) TiO_2 (Ti^{4+} with Ti $2p_{3/2}$ at ~ 458.7 eV); (b) Ti_2O_3 or $Ti_xO_yN_z$ (Ti^{3+} with Ti $2p_{3/2}$ at ~457.3 eV); and (c) TiO or TiN (Ti^{2+} with Ti $2p_{3/2}$ at ~455.5 eV). A similar procedure was carried out with the N 1s and O 1s core levels (not shown) but, except for the presence of N–Ti bonds (scaling with the nitrogen concentration of the films) and O=C bonds (due to unwanted surface contamination), their investigation provided no relevant information.

4. Discussion

In view of the adopted deposition conditions, most of the $Ti_xO_yN_z$ films present thicknesses in the 100–200 nm range and an optical transmittance at 632.8 nm (corresponding to the Raman laser excitation) below ~ 0.05. These figures suggest an optical (Raman) penetration depth of approx. 20 nm [24,25], that is larger than the layer thickness typically probed with the XPS measurements [26,27]. The only exception applies for film A, in which case (because of the deposition

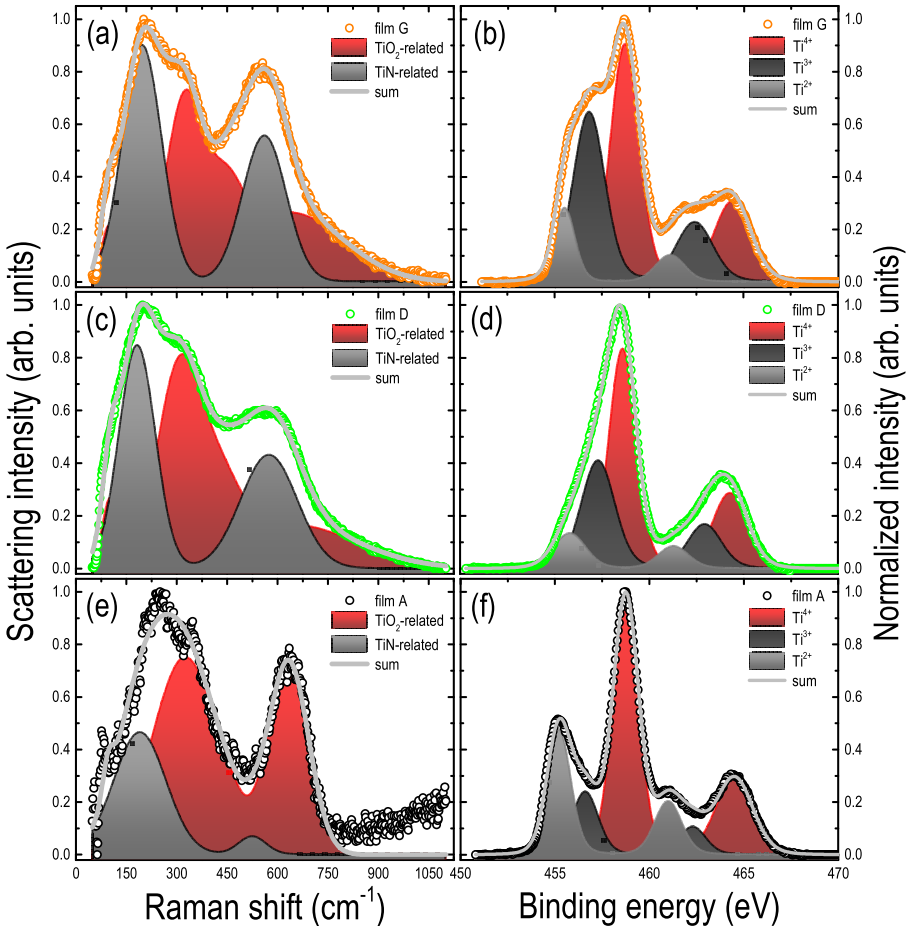

Fig. 2 – Raman scattering spectra and respective TiO_2- and TiN-related contributions present in $Ti_xO_yN_z$: (a) film G, (c) film D, and (e) film A (see Table 1). Ti 2p core levels ($2p_{3/2}$ and $2p_{1/2}$ components) according to the Ti^{4+}, Ti^{3+}, and Ti^{2+} chemical states of $Ti_xO_yN_z$: (b) film G, (d) film D, and (f) film A.

conditions) the film thickness was ~700 nm and no light transmittance at 632.8 nm was verified at all. Nevertheless, and apart from some adventitious surface contamination, the XPS data are very representative of the $Ti_xO_yN_z$ films and, as it will be shown, they are closely related to the Raman results.

The combined Raman-XPS data analysis starts with Fig. 3, that shows the areas of the TiO_2- and TiN-related phonon bands (see Fig. 2(a)–(c)–(e), for instance) as a function of the nitrogen and oxygen contents of the $Ti_xO_yN_z$ films (Table 1).

As can be seen, in spite of some data dispersion, the results make evident the linear relationship between the Raman spectra features (TiN- and TiO_2-related scattering signal areas) and the chemical composition of the $Ti_xO_yN_z$ films – as deposited according to different plasma atmospheres and TiO_2 and Ti targets. Moreover, the error bars were over-estimated in order to comply with both experimental (distinct scattering efficiencies) and data analysis (overlapping of nearby Raman signals) issues. Overall, the results of Fig. 3 corroborate not only the Raman-XPS data connection but, specially, the adopted Raman fitting procedure – as defined by the above-mentioned Gaussian-like (four TiO_2-related and two TiN-related) Raman bands, and respective phonon frequency values and tolerances.

To further explore the characteristics of the $Ti_xO_yN_z$ films, the effect of the atom composition onto the Ti-related chemical states was investigated as well. Hence, the fractions of Ti^{4+}, Ti^{3+}, and Ti^{2+} states present in the films are indicated in Fig. 4, as a function of the nitrogen and oxygen concentrations of the $Ti_xO_yN_z$ films. According to the figure, the most significant deviations apply to films deposited with the Ti target and, most probably, are due to the very high reactivity of Ti and characteristic surface sensitivity of XPS. On the other hand, considering the usual association of the Ti^{4+}, Ti^{3+}, and Ti^{2+} chemical states, respectively, to TiO_2, $Ti_xO_yN_z$, and TiN, the results of Fig. 4 are in perfect agreement with the nitrogen and oxygen measured concentrations.

An alternative representation of the data of Fig. 4 involves the sum of the fractions of Ti^{2+} and Ti^{3+} states (in a clear indication to the merging of TiN and $Ti_xO_yN_z$) and, as expected, produces the very same Ti^{2+}+Ti^{3+} slope of that exhibited by the Ti^{4+} states. In this case, however, the ensemble of results suggests the generation of TiN and/or $Ti_xO_yN_z$ at the expense of TiO_2. Anyway, and mainly because the XPS measurements were carried out with no sample

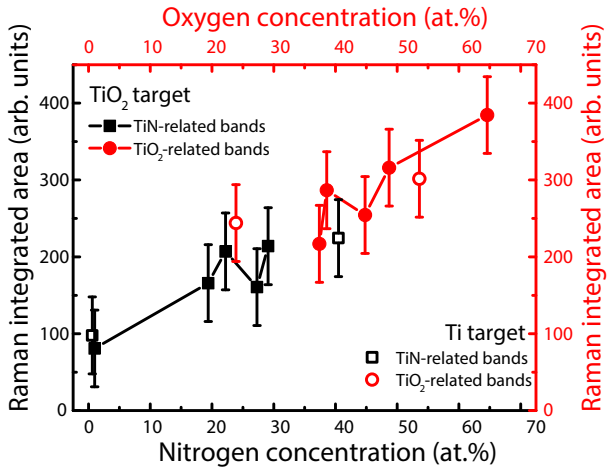

Fig. 3 – Raman integrated areas of the TiN- and TiO_2-related phonon bands present in radio frequency sputtered $Ti_xO_yN_z$ films. The data correspond to films deposited with TiO_2 (filled symbols) and Ti (open symbols) targets and show the correspondence of the Raman bands with the nitrogen (in black) and oxygen (in red) concentrations of the $Ti_xO_yN_z$ films. Error bars indicate typical data uncertainty. The solid lines joining the data points are just guides to the eye. (For interpretation of the references to color in this figure legend, the reader is referred to the Web version of this article.)

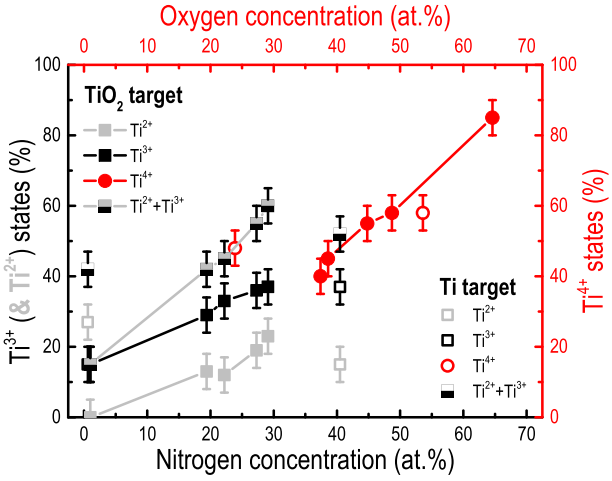

Fig. 4 – Ti^{4+}, Ti^{3+}, and Ti^{2+} chemical states (as provided by XPS data analysis) of rf sputtered $Ti_xO_yN_z$ films. The data correspond to films deposited with TiO_2 (filled symbols) and Ti (open and partially open symbols) targets and show how the Ti-related chemical states change with the nitrogen (in black and gray) and oxygen (in red) concentrations of the $Ti_xO_yN_z$ films. Error bars stand for average data uncertainty. The solid lines joining the data points are just guides to the eye. (For interpretation of the references to color in this figure legend, the reader is referred to the Web version of this article.)

cleaning, in its present form, the information contained in Fig. 4 clearly illustrates the systematic increasing (decreasing) percentage of Ti^{2+} and Ti^{3+} (Ti^{4+}) states with the insertion of nitrogen into the $Ti_xO_yN_z$ films.

Since the experimental results of Fig. 3 (Raman areas) and Fig. 4 (Ti-related chemical states) exhibit a mutual association with the nitrogen and oxygen concentrations of the $Ti_xO_yN_z$ films, it seems natural to examine how the phonon bands information correlates with the distribution of the Ti-related states. In order to proceed, the Raman data were considered in terms of their TiO_2- and TiN-related Raman area ratio ratios, *i.e.*: $TiO_2^{(ratio)} = (Area_{TiO_2})/(Area_{TiO_2} + Area_{TiN})$ and $TiN^{(ratio)} = (Area_{TiN})/(Area_{TiO_2} + Area_{TiN})$. These Raman ratios are shown in Fig. 5 as a function of their corresponding amounts of Ti^{4+} and $Ti^{2+}+Ti^{3+}$ chemical states.

The least square fittings of these experimental Raman-XPS data (with a goodness-of-fitting R-square ~ 0.62) are presented in Fig. 5 too. Based on them, it is possible to estimate the percentage of Ti-related states such that: $[Ti^{4+}] \sim 145 \times (TiO_2^{(ratio)} - 0.25)\%$ and $[Ti^{2+} + Ti^{3+}] \sim 145 \times (TiN^{(ratio)} - 0.06)\%$. The calculations are valid in the 0.15–0.85 Raman ratio range and involve a ~5% error.

The linear regression analysis was applied to the results of Fig. 3 as well. In this case, however, the absolute Raman-related areas were replaced by their corresponding TiO_2- and TiN-related Raman area ratios. The obtained expressions (R-square ~ 0.75) yield the oxygen and nitrogen contents of the $Ti_xO_yN_z$ films according to: $[O] \sim 123 \times (TiO_2^{(ratio)} - 0.27)$at.% and $[N] \sim 135 \times (TiN^{(ratio)} - 0.21)$at.%.

From the practical point of view, the importance of these Raman-XPS combined expressions is evident, especially when

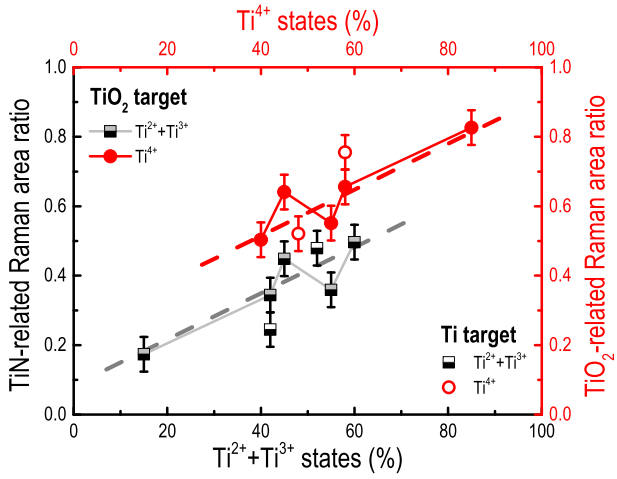

Fig. 5 – TiN- and TiO_2-related Raman ratios of $Ti_xO_yN_z$ films as a function of their corresponding Ti^{4+} and $Ti^{2+}+Ti^{3+}$ chemical states. Error bars denote typical uncertainties involving the Raman (±0.05) and the XPS (not shown, ~5%) data analysis. The dashed gray and red lines indicate the linear regression of the experimental data. (For interpretation of the references to color in this figure legend, the reader is referred to the Web version of this article.)

considering the speed and convenience in achieving high-quality Raman spectra at room environment – in contrast with the time and strict vacuum conditions required by the XPS measurements. Unfortunately, the use of the Raman bands (in its present form) allows to estimate the chemical aspects of the $Ti_xO_yN_z$ films only in a limited range and involves some uncertainty. On the other hand, additional films (involving more statistics and other compositions) certainly will contribute to improve the usefulness and precision of the method. Besides, as long as a typical 5% (absolute) error is satisfactory, the use of Raman analysis represents a very convenient approach to evaluate the chemical aspects of $Ti_xO_yN_z$ films. A similar procedure has been applied after thermal-induced crystallization of the considered $Ti_xO_yN_z$ films. In this case, however, the results indicate the complete transformation of $Ti_xO_yN_z$ into crystalline TiO_2 with its equivalent (expected) Ti^{4+}-related chemical states [28].

5. Concluding remarks

This paper reports on the properties of $Ti_xO_yN_z$ films, as provided by Raman scattering and X-ray photoelectron spectroscopy (XPS) measurements. In particular, it presents an original approach relating the Raman and XPS results with the purpose of establishing a connection between the atomic structure and the chemical states of $Ti_xO_yN_z$. The films were prepared by radio frequency sputtering TiO_2 and Ti solid targets according to different Ar + N_2 plasma atmospheres. Because of the deposition method the films present an amorphous + (nano/micro-)crystalline structure, and atom concentrations that scale with the deposition conditions. The detailed analysis of the Raman spectra indicates the presence of TiO_2-(at ~110, 300, 430 and 630 cm^{-1}) and TiN-related (at ~ 180 and 550 cm^{-1}) light scattering signals, that are perfectly consistent with the oxygen and nitrogen concentrations of the $Ti_xO_yN_z$ films. Likewise, the percentage of Ti^{4+}, Ti^{3+}, and Ti^{2+} chemical states (as determined from XPS) presents a clear relationship with the composition of the films as well as with their corresponding Raman TiO_2- and TiN-related bands. Altogether, this work shows the suitability of using the information provided by Raman spectroscopy to estimate the typical atom composition and Ti-related chemical states of $Ti_xO_yN_z$.

Funding

This work was financially supported by the Brazilian agencies CNPq and FAPESP (Project 2019/18460-4). ARZ and FA are CNPq fellows (Grants 303233/2017-6 & 302370/2015-3). FC and FGE are FAPESP fellows (Grants 2018/24461-0 & 2019/00757-0).

Declaration of Competing Interest

The authors declare that they have no known competing financial interests or personal relationships that could have appeared to influence the work reported in this paper.

REFERENCES

[1] See, for example Kageyama H, Hayashi K, Maeda K, Attfield JP, Hiroi Z, Rondinelli JM, et al. Expanding frontiers in materials chemistry and physics with multiple anions. Nature Commun 2018;9:772. https://doi.org/10.1038/s41467-018-02838-4. -7736.

[2] Yang X, Lin Y, Liu J, Liu W, Bi Q, Song X, et al. A highly conductive titanium oxynitride electron-selective contact for efficient photovoltaic devices. Adv Mater 2020;32. https://doi.org/10.1002/adma.202002608. 2002608-8pp.

[3] Asahi R, Morikawa T, Ohwaki T, Aoki K, Taga Y. Visible-light photocatalysis in nitrogen-doped titanium oxides. Science 2001;293:269–71. https://doi.org/10.1126/science.1061051.

[4] Trenczek-Zajac A, Radecka M, Zakrzewska K, Brudnik A, Kusior E, Bourgeois S, et al. Structural and electrical properties of magnetron sputtered Ti(ON) thin films: the case of TiN doped in situ with oxygen. J Power Sources 2009;194:93–103. https://doi.org/10.1016/j.jpowsour.2008.12.112.

[5] Singh A, Ahmed A, Sharma A, Sharma C, Paul S, Khosla A, et al. Promising photocatalytic degradation of methyl orange dye via sol-gel synthesized Ag-CdS@Pr-TiO_2 core/shell nanoparticles. Phys B Cond Matter 2021;616. https://doi.org/10.1016/j.physb.2021.413121. 413121-13pp.

[6] Musil J. Hard and superhard nanocomposite coatings. J Surf Coat Technol 2000;125:322–30. https://doi.org/10.1016/S0257-8972(99)00586-1.

[7] Naik GV, Schroeder JL, Ni X, Kildishev AV, Sands TD, Boltasseva A. Titanium nitride as a plasmonic material for visible and near-infrared wavelengths. Opt Mater Express 2012;2:478–89. https://doi.org/10.1364/OME.2.000478.

[8] Ramos R, Scoca D, Melo RB, Marques FC, Alvarez F, Zagonel LF. Study of nitrogen ion doping of titanium dioxide films. Appl Surf Sci 2018;443:619–27. https://doi.org/10.1016/j.apsusc.2018.02.259.

[9] See, for example Yoo JB, Yoo HJ, Jung HJ, Kim HS, Bang S, Choi J, et al. Titanium oxynitride microspheres with the rock-salt structure for use as visible-light photocatalysts. J Mater Chem A 2016;4:869–76. https://doi.org/10.1039/C5TA06758H.

[10] Scoca D, Morales M, Merlo RB, Alvarez F, Zanatta AR. Photoluminescence and compositional-structural properties of ion-beam sputter deposited Er-doped $TiO_{2-x}N_x$ films: their potential as a temperature sensor. J Appl Phys 2015;117. https://doi.org/10.1063/1.4921809. 205304-6pp.

[11] Echeverrigaray FG, Zanatta AR, Alvarez F. Reducible oxide and allotropic transition induced by hydrogen annealing: synthesis routes of TiO_2 thin films to tailor optical response. J Mater Res Technol 2021;12:1623–37. https://doi.org/10.1016/j.jmrt.2021.03.082.

[12] Scoca D, Cemin F, Bilmes SA, Figueroa CA, Zanatta AR, Alvarez F. Role of rare-earth elements and entropy on the Anatase-to-Rutile phase transformation of TiO_2 thin films deposited by ion beam sputtering. ACS Omega 2020;5:28027–36. https://doi.org/10.1021/acsomega.0c03431.

[13] Gouadec G, Colomban P. Raman spectroscopy of nanomaterials: how spectra relate to disorder, particle size and mechanical properties. Prog Cryst Growth Charact Mater 2007;53:1–56. https://doi.org/10.1016/j.pcrysgrow.2007.01.001.

[14] Engelhard MH, Droubay TC, Du Y. X-ray photoelectron spectroscopy applications, encyclopedia of spectroscopy and spectrometry. In: Lindon, editor. 3rd ed. Academic Press; 2017. p. 716–24. https://doi.org/10.1016/B978-0-12-409547-2.12102-X.

[15] Végh J. The Shirley background revised. J Electron Spectrosc Relat Phenom 2006;151:159–64. https://doi.org/10.1016/j.elspec.2005.12.002.
[16] Wagner CD, Davis LE, Zeller MV, Taylor ZA, Raymond RH, Gale LH. Empirical atomic sensitivity factors for quantitative analysis by electron spectroscopy for chemical analysis. Surf Interface Anal 1981;3:211–25. https://doi.org/10.1002/sia.740030506.
[17] http://www.casaxps.com/.
[18] See, for example Zanatta AR. A fast-reliable methodology to estimate the concentration of Rutile or Anatase phases of TiO_2. AIP Adv 2017;7:075201. https://doi.org/10.1063/1.4992130. -7pp.
[19] Naik VM, Haddad D, Naik R, Benci J, Auner GW. Optical properties of Anatase, Rutile and amorphous phases of TiO_2 thin films grown at room temperature by rf magnetron sputtering. MRS Proc 2002;755DD:11–2. https://doi.org/10.1557/PROC-755-DD11.12.
[20] Spengler W, Kaiser R, Christensen AN, Muller-Vogt G. Raman scattering, superconductivity, and phonon density of states of stoichiometric and non-stoichiometric TiN. Phys Rev B 1978;17:1095–101. https://doi.org/10.1103/PhysRevB.17.1095.
[21] Cheng YH, Tay BK, Lau SP, Kupfer H, Richter F. Substrate bias dependence of Raman spectra for TiN films deposited by filtered cathodic vacuum arc. J Appl Phys 2002;92:1845–9. https://doi.org/10.1063/1.1491588.
[22] Biesinger MC, Lau LW, Gerson AR, Smart RS. Resolving surface chemical states in XPS analysis of first row transition metals, oxides and hydroxides: Sc, Ti, V, Cu and Zn. Appl Surf Sci 2010;257:887–98. https://doi.org/10.1016/j.apsusc.2010.07.086.
[23] Jaeger D, Patscheider J. A complete and self-consistent evaluation of XPS spectra of TiN. J Electron Spectrosc Relat Phenom 2012;185:523–34. https://doi.org/10.1016/j.elspec.2012.10.011.
[24] See, for example Pankove JI. Optical processes in semiconductors. New York, NY: Dover Pub.; 1971, ISBN 0-486-60275-3 [Chapter 4].
[25] Nazari M, Holtz MW. Near-ultraviolet Raman and micro-Raman analysis of electronic materials. J Appl Phys 2018;5. https://doi.org/10.1063/1.5054660. 041303-20pp.
[26] Seah MP. Quantification of AES and XPS [Chapter 5]. In: Briggs D, Seah MP, editors. Practical surface analysis, auger and X-ray photoelectron spectroscopy, vol. 1. New York: Wiley; 1996. 0-471-95340-7.
[27] Powell CJ. Practical guide for inelastic mean free paths, effective attenuation lengths, mean escape depths, and information depths in x-ray photoelectron spectroscopy. J Vac Sci Technol A 2020;38. https://doi.org/10.1116/1.5141079. 023209-14pp.
[28] Zanatta AR, Echeverrigaray FG, Cemin, Alvarez F (unpublished results).